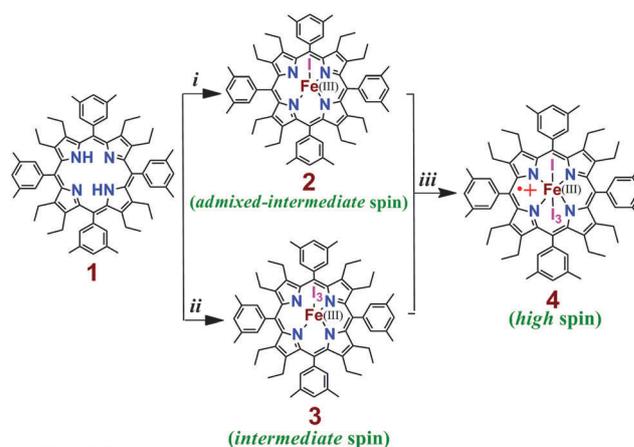# ChemComm

Controlled generation of highly saddled (porphyrinato)iron(III) iodide, tri-iodide and one-electron oxidized complexes†

Dipankar Sahoo and Sankar Prasad Rath*

For the first time, three iron(III) porphyrinato complexes have been synthesized selectively by varying the iodine concentration in the reaction mixture which eventually forms both five and six coordinate complexes with iodide and/or tri-iodide as axial ligands. Combined analysis using single crystal X-ray structure determination, and Mössbauer, ^{1}H NMR and EPR studies as well as VT magnetic studies has revealed the admixed-intermediate (iodo complex), pure intermediate (tri-iodide complex) and high-spin (1e-oxidized complex) states of iron.

Hemoproteins serve many diverse biological functions through the nearly identical heme prosthetic group as a consequence of the subtle coordination and redox chemistry apparent for iron porphyrins.[1–4] A variety of geometries, and oxidation and spin states of iron porphyrins, which are critical intermediates in the catalytic cycles of both biological and abiological systems, have been reproduced systematically using chemical models.[1–11] The spin states of five-coordinate iron(III) porphyrins are controlled mainly by the ligand field strength of axial ligands.[1,4–7] While most of the anionic ligands such as halides and hydroxides lead to the formation of high-spin ($S = 5/2$) complexes, extremely weak field ligands such as ClO_4 and SbF_6 give the complexes with quantum mechanical spin admixed states with varying proportions of pure $S = 3/2$ and $S = 5/2$ states. In fact, the degree of the $S = 3/2$ contribution fairly correlates with the ligand field strength of the anionic axial ligands when other factors are identical. In addition, the deformation of the porphyrin ring has also been known to influence the electronic structures of the iron(III) porphyrin complexes.[4–7] We report here the synthesis, X-ray structure and properties of three saddle distorted Fe(III) porphyrins generated *via* the controlled addition of iodine in the reaction mixture.

Department of Chemistry, Indian Institute of Technology Kanpur, Kanpur-208016, India. E-mail: sprath@iitk.ac.in; Fax: +91 512 259 7436; Tel: +91 512 259 7251

† Electronic supplementary information (ESI) available: Instrumentations, experimental details, spectroscopic characterizations, computational details, crystallographic data, Fig. S1–S13 and Tables S1–S4. CCDC 1419967 (**3**) and 1419968 (**2**). For ESI and crystallographic data in CIF or other electronic format see DOI: 10.1039/c5cc07111a

Free base octaethyltetraarylporphyrin **1** (Scheme 1) was prepared according to the literature procedure,[12] and the metal was inserted using excess FeI_2 in *N,N*-dimethylformamide under nitrogen. While washing the chloroform solution of the metal inserted complex with 1% HI in air forms the iodide complex **2**, the addition of 5% HI solution along with one equivalent iodine resulted in the formation of the tri-iodide complex **3**. Moreover, the addition of excess solid I_2 (5 equiv.) to either iodide (**2**) or tri-iodide complex (**3**) has produced the identical one-electron oxidized six-coordinate complex **4** where both iodide and tri-iodide occupy the fifth and sixth positions. Thus, **2**, **3** and **4** have been prepared by selectively varying the concentration of I_2 in the reaction mixture (Scheme 1). All the molecules have been isolated as a crystalline solid in high yields and two of them (**2** and **3**) are also structurally characterized. The UV-visible spectrum of **2** shows the Soret band at 416 nm in $CHCl_3$, while in **3**, the band shifted *via* a small blue shift to 413 nm along with a weak shoulder at 440 nm (Fig. 1). However, for the 1e-oxidized complex **4**, a blue-shifted broad Soret band appeared at 408 nm along with an intense shoulder peak at 442 nm. Typically, the electronic spectrum

Conditions:

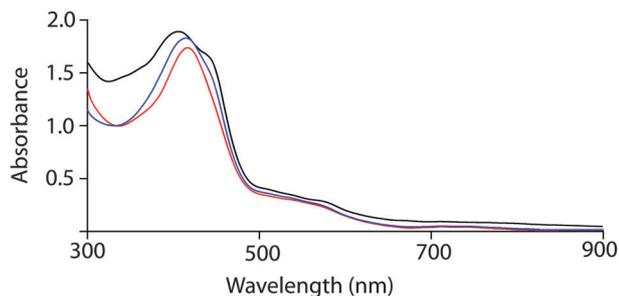*i*: FeI_2 + 1% HI; *ii*: FeI_2 + 5 % HI + I_2 (1 eqv); *iii*: I_2 (5 eqv)

Scheme 1

Fig. 1 UV-visible spectra (in CHCl$_3$ at 295 K) using polycrystalline samples of **2** (red line), **3** (blue line) and **4** (black line).
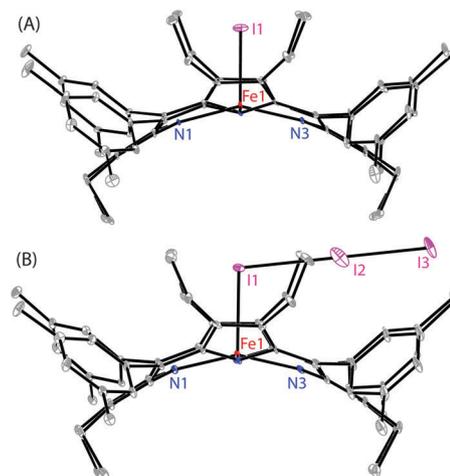

Fig. 2 Perspective views (at 100 K) of (A) **2** and (B) **3** showing 50% thermal contours for all non-hydrogen atoms (H atoms have been omitted for clarity). Selected bond distances (Å) and angles (deg) for **2**: Fe1–N1, 1.977(4); Fe1–N2, 1.999(4); Fe1–N3, 1.976(4); Fe1–N4, 2.001(4); Fe1–I1, 2.5236(10); N1–Fe1–N2, 88.08(16); N1–Fe1–N4, 88.36(16); N2–Fe1–N4, 151.14(17); N3–Fe1–N1, 167.06(17); N3–Fe1–N2, 88.36(17); N3–Fe1–N4, 88.76(17); N1–Fe1–I1, 96.26(12); N2–Fe1–I1, 105.51(12); N3–Fe1–I1, 96.69(12); N4–Fe1–I1, 103.35(12). For **3**: Fe1–N1, 1.932(6); Fe1–N2, 1.975(10); Fe1–N3, 1.951(9); Fe1–I1, 2.7503(19); I1–I2, 3.0164(14); N1–Fe1–N2, 89.53(19); N3–Fe1–N1, 89.42(19); N3–Fe1–N2, 158.3(4); N1–Fe1–I1, 92.8(2); N2–Fe1–I1, 101.4(3); N3–Fe1–I1, 100.4(3); I1–I2–I3, 173.87(5).

characteristics of a radical cation species are a new band at low energy and a dramatically broadened, blue-shifted Soret band relative to the unoxidized species.[8] Here, **4** displays the characteristic features of π-cation radicals. However, the near-IR band, which is associated with the formation of a dimeric π-cation radical, has not been observed in **4** due to the formation of the six-coordinate complex. The oxidized complex showed the IR marker bands[8] characteristic for a porphyrin π-cation radical at 1596 and 1448 cm^{-1} which indicate the formation of a π-cation radical in the complex (Fig. S1, ESI†). The electrospray ionization mass spectrometry (ESI-MS) showed intense peaks at m/z 1131.4481 for [**2**]$^+$, 1385.6151 for [**3**]$^+$, and 1512.1478 for [**4**]$^+$ (Fig. S2–S4, ESI†) confirming the formation of the complexes. The isotopic distribution patterns of the experimental mass were also nicely correlated with the calculated patterns.

Dark-purple crystals of **2** and **3** were grown by slow diffusion of cyclohexane and acetonitrile, respectively, into the solution of the respective complex in chloroform at room temperature in air.[13] Dark-purple crystals of the oxidized complex **4** were also obtained by slow diffusion of hexane into the chloroform solution of the complex. However, the highly disordered nature of the I$_3$ axial ligand failed to provide a good quality structure of the complex. The perspective views of **2** and **3** are shown in Fig. 2 (and see Fig. S5 and S6 (ESI†) for the molecular packing diagrams). In the X-ray structure (Tables S1 and S2, ESI†), the iron centers have a five-coordinate square-pyramidal geometry and have shown considerable doming of the porphyrin cores. The Fe–I bond undergoes an extensive elongation from a distance of 2.5236(10) Å in **2** to 2.7503(19) Å in the tri-iodide complex **3** which is also indicative of a weaker ligand field strength of the tri-iodide ion. Also, the average Fe–Np distances in the two types of complexes are different: 1.988(4) Å in **2** and 1.947(8) Å in **3**. As can be seen, the Fe–I distance increases as the bond distance of Fe–Np decreases. The displacement of the iron center from the mean plane of the C$_{20}$N$_4$ porphyrinato core (Δ_{24}^{Fe}) is contracted from 0.36 Å (in **2**) to 0.21 Å (in **3**). All these structural features are characteristic for having admixed-intermediate and pure intermediate spin ($S = 3/2$) states of iron, respectively, in **2** and **3**.[4–11] In contrast, iron centers are mostly high-spin in all the previously reported iodo complexes (Table S3, ESI†) that are structurally characterized.[9] Also, porphyrin rings are highly distorted in **2** and **3** and assume a nearly pure saddle shape (Fig. S7 and S8, ESI†).

Mössbauer parameters are one of the most powerful probes to determine the spin state of the iron(III) porphyrins.[5,7a,8] Fig. 3 compares the Mössbauer spectra of the microcrystalline samples of **2**, **3**, and **4** at 100 K. Complexes **2** and **3** have displayed a doublet with a large quadrupole-splitting [δ(ΔE$_q$): 0.35 (3.42) mm s^{-1} for **2** and 0.37 (3.80) mm s^{-1} for **3**] characteristic of an admixed-intermediate and a pure intermediate ($S = 3/2$) state of iron, respectively. In contrast, 1e-oxidized complex **4** exhibits a broad doublet with a small quadrupole-splitting from which the IS and QS values are determined to be 0.27 and 0.74 mm s^{-1}, respectively, which fall within the range of the parameters known for high-spin ($S = 5/2$) Fe(III) porphyrins.

To obtain much conclusive evidence for the spin state, the EPR spectroscopic measurements were carried out for the complexes in both solid and solution phases (Fig. S9, ESI†). The spectra were carefully simulated (a representative simulated spectrum is shown in Fig. S10, ESI†). All the spectra are axially symmetric with $g_\perp$ = 4.24 and $g_\parallel$ = 1.99 for **2**, and $g_\perp$ = 4.05 and $g_\parallel$ = 2.01 for **3** at 77 K in the solid state. Similar g values are also obtained for the molecules in solution. In the case of **2**, hyperfine coupling of 50.8 G has clearly been observed at $g = 2$ with the axially coordinated iodide. The contributions of the $S = 3/2$ spin state can be estimated as $(6 - g_\perp)/2$,[5] which are calculated to be 88% and 98% for **2** and **3**, respectively. Consistent with the X-ray structure, and SQUID and Mössbauer results, **3** shows a quite pure $S = 3/2$ spin state.

^{1}H NMR spectroscopy is a valuable tool to distinguish different spin states of iron(III) porphyrins in solution.[4,7,10,11,14] Fig. 4 shows the spectra of **2**, **3** and **4** recorded at 295 K in CDCl$_3$. The ^{1}H NMR chemical shifts between **2** and **3** exhibit some differences depending on the axial ligand strengths.
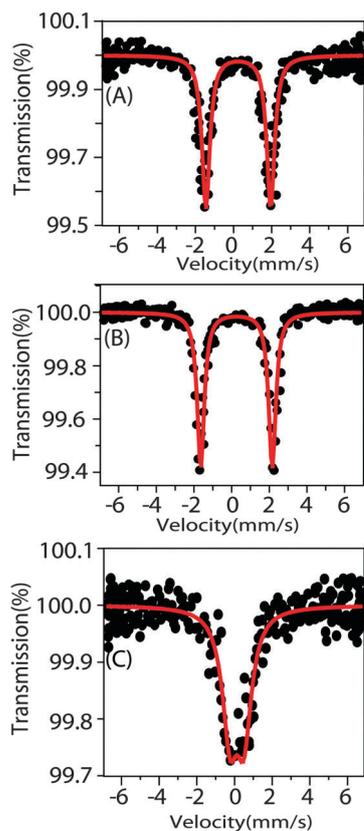
Fig. 3 Mössbauer spectra of (A) **2**, (B) **3**, and (C) **4** at 100 K.

Fig. 4 ^{1}H NMR spectra of (A) **2**, (B) **3**, and (C) **4** at 295 K in CDCl$_3$.

For complex **2**, four methylene proton signals are observed at 48.81, 32.15, 30.15, and 15.06 ppm (average 31.54 ppm) which are similar to those of the five-coordinate iron(III) iodo complex with the admixed-intermediate spin states reported earlier.[14a] In complex **3**, however, four methylene peaks are observed at 42.25, 14.09, 12.85, and 9.45 ppm (average 19.66 ppm) and are characteristic of pure intermediate spin states.[7,11] Thus, upon moving from an iodo to a tri-iodide complex, the spin state of iron has been changed from a admixed-intermediate state to a pure intermediate state.

For a one-electron oxidized complex **4**, four methylene proton signals are observed at 87.06, 14.07 and 10.28 (2) ppm which are, however, characteristic of the high-spin state of iron.[4,7a] Interestingly, the *ortho* and *para* proton signals of the phenyl substituents are observed at 30.29, 28.09 and 36.65 ppm, respectively, (Fig. 4C) which indicates the presence of a_{2u} porphyrin π-cation radicals.[14b] A characteristic feature of this type of radical is the large spin densities on the *meso* carbons which induce large isotropic shifts of the *meso* phenyl protons in the ^{1}H NMR spectrum as exemplified by the extremely downfield-shifted *ortho* and *para* protons and upfield-shifted *meta* signals.[4,14] The result also indicates that **4** has a negative spin density at the *meso* carbon atoms caused by the antiferromagnetic coupling between the paramagnetic iron and the a_{2u} radical spin.[14] The oxidation has also induced a wider separation between up-field- and down-field-shifted CH$_2$ signals which can be explained to be due to the formation of π-cation radicals along with a change of iron spin state from $S = 3/2$ to $5/2$.
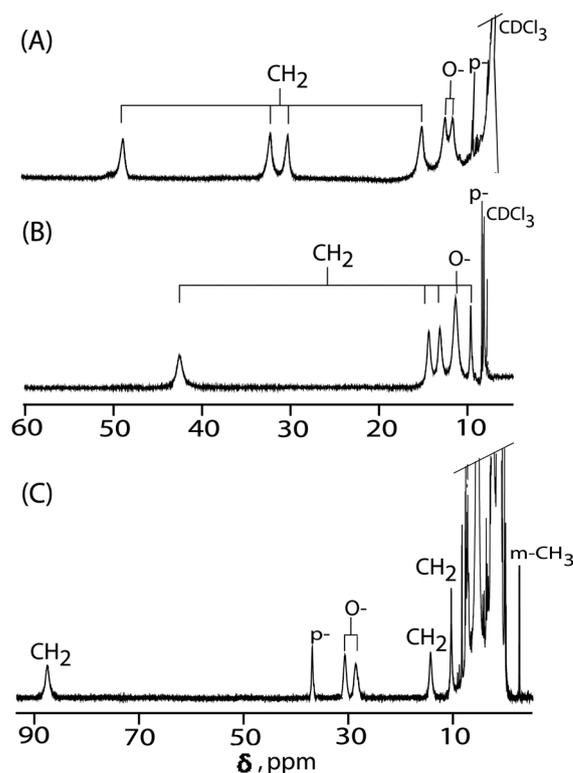
Variable-temperature magnetic susceptibility measurements has been carried out in the solid state for 1e-oxidized complex **4**, and was fit (Fig. S11, ESI†) using the software PHI.[15] The iron(III) center was treated as a high spin ($S = 5/2$) with a g value set at 2.0 and the presence of a small amount of residual iron(III) impurity was also taken into consideration. The coupling between the iron spin and the porphyrin radical does show a significant value ($-J_{Fe-r} = 62.8$ cm^{-1}). The inter-ring coupling that is closely related only to the degree of the ring overlap[8a] has not been considered due to the six-coordinate nature of the complex. Also, the near-IR band, which is associated with the formation of a dimeric π-cation radical,[8] has not been observed in **4**. The a_{2u} radical wave function has a large amplitude at the pyrrole nitrogens, and thus it is expected that the a_{2u} orbital overlaps strongly with the iron d-orbitals which resulted in a larger iron–radical coupling.[14,16]

To gain insight into the origin of the spin-state, we ran a series of density functional theory calculations on **3** and **4** (see the ESI† for details) considering both high ($S = 5/2$) and intermediate spin ($S = 3/2$) states of iron in each case. Geometry optimisations were carried out using respective spin multiplicities: quartet and sextet states for **3** while triplet (considering an antiferromagnetic inter-action between the π-cation radical and the intermediate spin of iron(III)) and quintet (considering an antiferromagnetic coupling between the π-cation radical and the high-spin of iron(III)) states for **4**. The optimized geometries of **3** and **4** are shown in Fig. 5. As can be seen, the optimized geometries of ^{4}**3** match the crystal structure coordinates reasonably well. Also, **3** has been found to be stabilized in an intermediate-spin (IS) state with $\Delta G_{HS/IS} = 10.63$ kcal mol^{-1} as compared to the high-spin (HS) state.
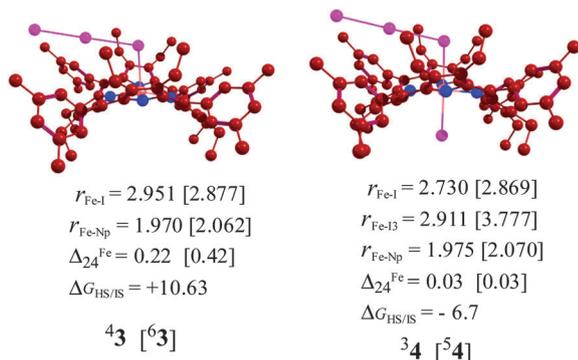
$r_{\text{Fe-I}} = 2.951\ [2.877]$
$r_{\text{Fe-Np}} = 1.970\ [2.062]$
$\Delta_{24}^{\text{Fe}} = 0.22\ [0.42]$
$\Delta G_{\text{HS/IS}} = +10.63$

$^{4}\mathbf{3}\ [^{6}\mathbf{3}]$

$r_{\text{Fe-I}} = 2.730\ [2.869]$
$r_{\text{Fe-I3}} = 2.911\ [3.777]$
$r_{\text{Fe-Np}} = 1.975\ [2.070]$
$\Delta_{24}^{\text{Fe}} = 0.03\ [0.03]$
$\Delta G_{\text{HS/IS}} = -6.7$

$^{3}\mathbf{4}\ [^{5}\mathbf{4}]$

Fig. 5 UB3LYP/BS1 optimized geometries of $^{4,6}\mathbf{3}$ and $^{3,5}\mathbf{4}$ with bond lengths (r) in Å. Δ_{24}^{Fe} is the average displacement (in Å) of the metal from the least-square plane of the $C_{20}N_4$ porphyrinato core. Free energies $\Delta G_{\text{HS/IS}}$ are relative to the intermediate spin state in kcal mol^{-1}.

In contrast, the addition of two axial ligands iodide and tri-iodide changes the spin state ordering in **4** and stabilizes the high-spin state ($\Delta G_{\text{HS/IS}} = -6.7$ kcal mol^{-1}) of iron.

Studies on model hemes suggest that the intermediate-spin state is critically dependent on the axial ligand strength. Tri-iodide is a weaker axial ligand compared to iodide, which is, however, responsible for the stabilization of the admixed intermediate and pure intermediate spin states of iron in **2** and **3**, respectively, as demonstrated here. Both the molecules, although looking very similar, are carefully isolated and structurally characterized which enable us to investigate their spectroscopic identities that were missing so far. Moreover, the one-electron oxidized six-coordinate complex **4** stabilizes the high-spin state of iron with iodide and tri-iodide as axial ligands and has been formulated as the iron(III) porphyrin π-cation radical. A variable temperature magnetic study in solids has shown a strong antiferromagnetic coupling between iron and radical spins in the oxidized complex **4**. Furthermore, computational calculations clearly support the experimentally assigned spin state.

For the first time, three iron(III) porphyrinato complexes have been synthesized selectively just by slight variations of the iodine concentration in the reaction mixture which eventually forms both five- and six-coordinate complexes with iodide and/or tri-iodide as axial ligands. Single crystal X-ray structure determination, and Mössbauer, ^{1}H NMR and EPR studies as well as VT magnetic studies have revealed their electronic structure and properties. Iodine is not known to be a strong oxidant; however, axial coordination of iodide/tri-iodide in **2/3** enables the facial oxidation of the complexes using iodine to form the iron(III) porphyrin π-cation radical **4**. The present work also highlights the various roles of iodine and opportunities therein in chemical synthesis. Further work is in progress.

Notes and references

1 W. R. Scheidt, in *The Porphyrin Handbook*, ed. K. M. Kadishi, K. M. Smith and R. Guilard, Academic Press, San Diego, 2000, vol. 3, pp. 49–112.
2 (*a*) J. A. Shelnutt, X.-Z. Song, J.-G. Ma, S.-L. Jia, W. Jentzen and C. J. Medforth, *Chem. Soc. Rev.*, 1998, **27**, 31–42; (*b*) M. O. Senge, *Chem. Commun.*, 2006, 243.
3 (*a*) F. A. Walker, *Chem. Rev.*, 2004, **104**, 589–615; (*b*) F. A. Walker, *Coord. Chem. Rev.*, 1999, **185–186**, 471–534.
4 (*a*) A. Ikezaki, Y. Ohgo and M. Nakamura, *Coord. Chem. Rev.*, 2009, **253**, 2056–2069; (*b*) M. Nakamura, *Coord. Chem. Rev.*, 2006, **250**, 2271–2294.
5 (*a*) R. Weiss, A. Gold and J. Terner, *Chem. Rev.*, 2006, **106**, 2550–2579; (*b*) Y. Ling and Y. Zhang, *J. Am. Chem. Soc.*, 2009, **131**, 6386–6388.
6 (*a*) C. A. Read and F. Guiset, *J. Am. Chem. Soc.*, 1996, **118**, 3281–3282; (*b*) R. J. Cheng, P. Y. Chen, P. R. Gau, C. C. Chen and S. M. Peng, *J. Am. Chem. Soc.*, 1997, **119**, 2563–2569.
7 (*a*) D. Sahoo, M. G. Quesne, S. P. de Visser and S. P. Rath, *Angew. Chem., Int. Ed.*, 2015, **54**, 4796–4800; (*b*) S. Bhowmik, S. K. Ghosh and S. P. Rath, *Chem. Commun.*, 2011, **47**, 4790–4792; (*c*) S. K. Ghosh, R. Patra and S. P. Rath, *Inorg. Chem.*, 2010, **49**, 3449–3460.
8 (*a*) M. Li, T. J. Neal, G. R. A. Wyllie, C. E. Schulz and W. R. Scheidt, *Inorg. Chem.*, 2010, **49**, 8078–8085; (*b*) M. Li, T. J. Neal, G. R. A. Wyllie, A. G. Oliver, C. E. Schulz and W. R. Scheidt, *Inorg. Chem.*, 2011, **50**, 9114–9121; (*c*) S. Hu and T. G. Spiro, *J. Am. Chem. Soc.*, 1993, **115**, 12029–12034.
9 (*a*) Y. Ohgo, S. Neya, M. Takahashi, M. Takeda, N. Funasaki and M. Nakamura, *Chem. Lett.*, 2003, **32**, 526–527; (*b*) K. Hatano and W. R. Scheidt, *Inorg. Chem.*, 1979, **18**, 877–879; (*c*) Y. Ohgo, S. Neya, T. Ikeue, M. Takahashi, M. Takeda, N. Funasaki and M. Nakamura, *Inorg. Chem.*, 2002, **41**, 4627–4629.
10 (*a*) R. Patra, D. Sahoo, S. Dey, D. Sil and S. P. Rath, *Inorg. Chem.*, 2012, **51**, 11294–11305; (*b*) R. Patra, S. Bhowmik, S. K. Ghosh and S. P. Rath, *Dalton Trans.*, 2010, **39**, 5795–5806; (*c*) R. Patra, A. Chaudhury, S. K. Ghosh and S. P. Rath, *Inorg. Chem.*, 2008, **47**, 8324–8335; (*d*) R. Patra and S. P. Rath, *Inorg. Chem. Commun.*, 2009, 515–519.
11 (*a*) D. Sil and S. P. Rath, *Dalton Trans.*, 2015, **44**, 16195–16211; (*b*) M. A. Sainna, D. Sil, D. Sahoo, B. Martin, S. P. Rath, P. Comba and S. P. de Visser, *Inorg. Chem.*, 2015, **54**, 1919–1930; (*c*) D. Sil, F. S. T. Khan and S. P. Rath, *Inorg. Chem.*, 2014, **53**, 11925–11936; (*d*) S. K. Ghosh, S. Bhowmik, D. Sil and S. P. Rath, *Chem. – Eur. J.*, 2013, **19**, 17846–17859; (*e*) S. Bhowmik, S. Dey, D. Sahoo and S. P. Rath, *Chem. – Eur. J.*, 2013, **19**, 13732–13744; (*f*) S. Bhowmik, S. K. Ghosh, S. Layek, H. C Verma and S. P. Rath, *Chem. – Eur. J.*, 2012, **18**, 13025–13037; (*g*) S. K. Ghosh and S. P. Rath, *J. Am. Chem. Soc.*, 2010, **132**, 17983–17985; (*h*) S. K. Ghosh, R. Patra and S. P. Rath, *Inorg. Chim. Acta*, 2010, **363**, 2791–2799.
12 K. M. Barkigia, M. D. Berber, J. Fajer, C. J. Medforth, M. W. Renner and K. M. Smith, *J. Am. Chem. Soc.*, 1990, **112**, 8851–8857.
13 Crystal data for **2**: orthorhombic, space group *Pbca*, *Z* = 8, *a* = 19.736(5) Å, *b* = 24.456(5) Å, *c* = 31.304(5) Å, *V* = 15109(5) Å³. *d*$_{\text{calcd}}$ = 1.014 Mg m^{-3}. *R*$_1$ = 0.0888, w*R*$_2$ (all data) = 0.2583. Goodness of fit on *F*² = 1.034. For **3** orthorhombic, space group *Pnma*, *Z* = 1, *a* = 23.387(5) Å, *b* = 17.301(4) Å, *c* = 18.913(4) Å, *V* = 7653(3) Å³. *d*$_{\text{calcd}}$ = 1.410 mg m^{-3}. *R*$_1$ = 0.0740, w*R*$_2$ (all data) = 0.2379. Goodness of fit on *F*² = 1.046. CCDC 1419968, and 1419967 contains the supplementary crystallographic data of **2** and **3**, respectively, for this paper.
14 (*a*) M. Nakamura, T. Ikeue, Y. Ohgo, M. Takahashi and M. Takeda, *Chem. Commun.*, 2002, 1198–1199; (*b*) S. Kouno, A. Ikezaki, T. Ikeue and M. Nakamura, *J. Inorg. Biochem.*, 2011, **105**, 718–721.
15 N. F. Chilton, R. P. Anderson, L. D. Turner, A. Soncini and K. S. Murray, *J. Comput. Chem.*, 2013, **34**, 1164–1175.
16 (*a*) T. Vangberg, R. Lie and A. Ghosh, *J. Am. Chem. Soc.*, 2002, **124**, 8122–8130; (*b*) H. Hirao, S. Shaik and P. M. Kozlowski, *J. Phys. Chem. A*, 2006, **110**, 6091–6099; (*c*) R.-J. Cheng, P.-Y. Chen, T. Lovell, T. Liu, L. Noodleman and D. A. Case, *J. Am. Chem. Soc.*, 2003, **125**, 6774–6783.